

# Giant Spin-Hall Effect Induced by the Zeeman Interaction in Graphene

D. A. Abanin,<sup>1</sup> R. V. Gorbachev,<sup>2</sup> K. S. Novoselov,<sup>2</sup> A. K. Geim,<sup>2</sup> and L. S. Levitov<sup>3</sup>

<sup>1</sup>*Princeton Center for Theoretical Science and Department of Physics, Princeton University, Princeton, New Jersey 08544, USA*

<sup>2</sup>*Manchester Centre for Mesoscience and Nanotechnology, University of Manchester, Manchester M13 9PL, United Kingdom*

<sup>3</sup>*Department of Physics, Massachusetts Institute of Technology, Cambridge, Massachusetts 02139, USA*

(Received 21 March 2011; published 23 August 2011)

We propose a new approach to generate and detect spin currents in graphene, based on a large spin-Hall response arising near the neutrality point in the presence of an external magnetic field. Spin currents result from the imbalance of the Hall resistivity for the spin-up and spin-down carriers induced by the Zeeman interaction, and do not involve a spin-orbit interaction. Large values of the spin-Hall response achievable in moderate magnetic fields produced by on-chip sources, and up to room temperature, make the effect viable for spintronics applications.

DOI: 10.1103/PhysRevLett.107.096601

PACS numbers: 72.80.Vp, 72.15.Gd

The spin-Hall effect (SHE) is a transport phenomenon resulting from the coupling of spin and charge currents: an electrical current induces a transverse spin current and vice versa [1,2]. The SHE offers tools for electrical manipulation of electron spins via current-induced spatial segregation of carriers with opposite spin [3,4]. All SHE mechanisms known to date rely on the spin-orbit interaction. The two main varieties of SHE, intrinsic and extrinsic, arise due to spin-orbit terms in the band Hamiltonian [5] and spin-dependent scattering on impurities [1], respectively.

Single layer graphene has emerged recently as an attractive material for spintronics that features long spin diffusion lengths [6], gate tunable spin transport [6,7], and high-efficiency spin injection [8]. However, to realize the full potential of graphene, several issues must be addressed. First, the measured spin lifetimes are orders of magnitude shorter than theoretical predictions [6–11] calling for identifying and controlling extrinsic mechanisms of spin scattering [10–14]. Second, the low intrinsic spin-orbit coupling values [9,15] render the conventional SHE mechanisms ineffective, depriving graphene spintronics of a crucial control knob for spin transport.

Here we outline a new approach to generate and probe spin currents in graphene, based on a SHE response in the presence of magnetic field that does not rely on spin-orbit interaction. Spin currents are generated by the combined effect of spin and orbital coupling to magnetic field. The Zeeman splitting lifts spin degeneracy and imbalances the Hall resistivities of different spin species (see Fig. 1 inset), leading to a net transverse spin current in response to an applied charge current. The resulting SHE response, called below ZSHE for brevity, is an essentially classical effect that offers a robust and efficient way to generate spin currents. The ZSHE response is sharply enhanced near the Dirac point (DP). Unlike the proposals relying on a spin gap opened in the graphene bulk by spin-orbital or Zeeman interactions [16,17], where temperatures are

constrained by the spin gap values,  $k_B T < \Delta$ , the ZSHE mechanism can operate in a wide range of temperatures and magnetic fields. This makes the effect viable for spintronics applications, such as spin sources and spin injection that do not rely on magnetic contacts.

The enhancement at the DP, which results from special transport properties of the Dirac fermions, is illustrated in Fig. 1. Transport is unipolar at high doping from the DP, dominated by carriers of one type, with  $\rho_{xy}$  following the standard quasiclassical expression,

$$\rho_{xy}(n) = -\frac{B}{nec}. \quad (1)$$

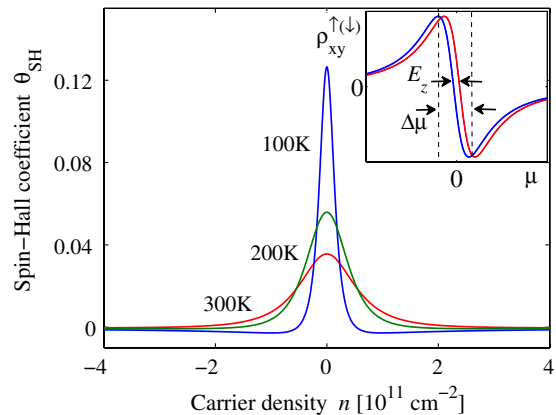


FIG. 1 (color online). Spin-Hall response induced by an external magnetic field in graphene in the absence of spin-orbit coupling. The SHE coefficient  $\theta_{SH}$ , Eq. (3), peaks at the Dirac point (DP). Spin currents at the DP originate from the imbalance of the spin-up and spin-down Hall resistivities due to Zeeman splitting  $E_Z$  (inset, red and blue curves). Steep behavior of  $\rho_{xy}$  “amplifies” the effect of Zeeman splitting, resulting in a large spin-Hall response for  $|\mu| \lesssim \Delta\mu$ . Large values  $\theta_{SH}$  can be reached already at moderate field strengths and high temperatures, Eq. (14). Parameters used are  $B = 1$  T, disorder broadening  $\gamma = 100$  K, electron-hole drag coefficient  $\eta = 2.3\hbar$ .

Transport near the DP is bipolar, which produces smearing of the  $1/n$  singularity in  $\rho_{xy}$  by the effects of two-particle scattering as well as disorder. This leads to a steep linear dependence in  $\rho_{xy}(n)$  at the DP (Fig. 1 inset), which is also seen in experiment (Fig. 3). The large values of  $\partial\rho_{xy}/\partial n$ , despite the smallness of the Zeeman splitting, can yield giant ZSHE response.

The conventional SHE is described by the spin-Hall conductivity which relates transverse spin current and the electric field [1,2]. To identify the relevant quantity for ZSHE, we consider spin accumulation in the situation when the two spin species are independent, each described by its own conductivity tensor. For a strip carrying uniform current [Fig. 2(a)], the transverse gradients of electrochemical potential for each spin projection are

$$\nabla_y \left( \phi + \frac{n_{\uparrow}}{e\nu_{\uparrow}} \right) = \frac{\rho_{xy}^{\uparrow}}{\rho_{xx}^{\uparrow}} \mathcal{E}, \quad \nabla_y \left( \phi + \frac{n_{\downarrow}}{e\nu_{\downarrow}} \right) = \frac{\rho_{xy}^{\downarrow}}{\rho_{xx}^{\downarrow}} \mathcal{E}, \quad (2)$$

where  $\mathcal{E}$  is the electric field  $x$  component and  $n_{\uparrow(\downarrow)}$  and  $\nu_{\uparrow(\downarrow)}$  are the spin-up (spin-down) concentration and density of states. Ignoring spin relaxation, we estimate spin density at the edge  $n_s = n_{\uparrow} - n_{\downarrow}$  as

$$n_s = \frac{\theta_{SH} w e \mathcal{E}}{\nu_{\uparrow}^{-1} + \nu_{\downarrow}^{-1}}, \quad \theta_{SH} = \frac{\rho_{xy}^{\uparrow}}{\rho_{xx}^{\uparrow}} - \frac{\rho_{xy}^{\downarrow}}{\rho_{xx}^{\downarrow}} \approx E_Z \frac{\partial \rho_{xy}}{\partial \mu \rho_{xx}}, \quad (3)$$

with  $E_Z$  the Zeeman splitting (for full treatment, see [18]). Here we used the smallness of  $E_Z$  compared to the DP smearing  $\Delta\mu$  (see Fig. 1) to express  $\theta_{SH}$  as a derivative with respect to  $\mu$ . We see that the quantity  $\theta_{SH}$  plays a role identical to the ratio of the spin-Hall and Ohmic

conductivities  $\xi_{SH} = 2\sigma_{SH}/\sigma_{xx}$  in the conventional SHE. We will thus refer to  $\theta_{SH}$  as the SHE coefficient.

For realistic parameter values, Eq. (3) yields large  $\theta_{SH}$  at the peak (see Fig. 1). For  $B = 1$  T, using disorder strength estimated from mobility in graphene on a BN substrate,  $\gamma \approx 100$  K [see Eq. (10)], we find  $\theta_{SH} = 0.1$ . This is more than 2 orders of magnitude greater than the SHE values in typical spintronics materials with spin-orbit SHE mechanism. Say, we estimate  $\xi_{SH} \approx 5 \times 10^{-4}$  from the spin and charge resistance measured in an InGaAs system [4]. The “giant” values  $\theta_{SH}$  are in fact to be expected, since the ZSHE can be viewed as a classical counterpart of the SHE at  $k_B T < E_Z$  discussed in Refs. [17,19] characterized by quantized  $\sigma_{SH} = 2e^2/h$ .

Large  $\theta_{SH}$  values result in “giant” spin accumulation. From Eq. (3), taking  $\theta_{SH} = 0.1$  and the density of states at disorder-broadened DP  $\nu_{\uparrow(\downarrow)} \approx \sqrt{\Delta n}/\pi\hbar v_0$  (with density inhomogeneity  $\Delta n \approx 10^{10} \text{ cm}^{-2}$  typical for graphene on BN substrate [20]), and using  $\mathcal{E} = 1 \text{ V}/\mu\text{m}$  (a maximum field for which transport is Ohmic [21]), we estimate  $n_s$  at the edges of a  $2 \mu\text{m}$ -wide graphene strip:

$$n_s \approx 3 \times 10^9 \text{ cm}^{-2}, \quad (4)$$

which is comparable to the DP width  $\Delta n$ . Such large densities can be easily detected by spin-dependent tunneling. The estimate (4) is also 4 orders of magnitude greater than the spin accumulation per atomic layer observed in a three-dimensional GaAs [4],  $n_s \approx 5 \times 10^5 \text{ cm}^{-2}$ .

Another attractive feature of the ZSHE is that it can enable local generation and detection of spin currents. Permanent micromagnets can generate fields up to 1 T concentrated to regions of size  $\sim 0.5 \mu\text{m}$  [22] (fields up to 1.4 T are achievable using widely available neodymium boron magnets). State-of-the-art microelectromagnets used in read/write heads of hard disk drives can generate a very strong and spatially localized magnetic field, reaching 0.5 T in areas around  $100 \text{ nm} \times 35 \text{ nm}$ . In an H-shaped device, pictured in Fig. 2(b), spin currents can be generated on one end of a graphene strip and detected on the opposite end. External  $B$  field can be used to induce spin precession which will manifest itself in Hanle-type oscillations of the voltage measured between probes 3 and 4. This setup can serve as an all-electric probe of spin currents [20,23,24].

To model the dependence of  $\theta_{SH}$  on  $B$ ,  $T$ , and disorder, we employ the quantum kinetic equation approach of Refs. [25,26]. To describe transport near the DP, it is crucial to account for the contributions of both electrons and holes. For a spatially uniform system, we have

$$q_{e(h)} \left( \mathbf{E} + \frac{\mathbf{v}}{c} \times \mathbf{B} \right) \frac{\partial f_{e(h)}(\mathbf{p})}{\partial \mathbf{p}} = \text{St}[f_e(\mathbf{p}), f_h(\mathbf{p})], \quad (5)$$

where  $f_{e(h)}(\mathbf{p})$  is the distribution function for electrons and holes, and  $q_e = -q_h = e$ . The collision integral describes two-particle collisions and scattering by disorder [25,26]. The approach based on Eq. (5) is valid in the quasiclassical regime, when particle mean free paths are long compared

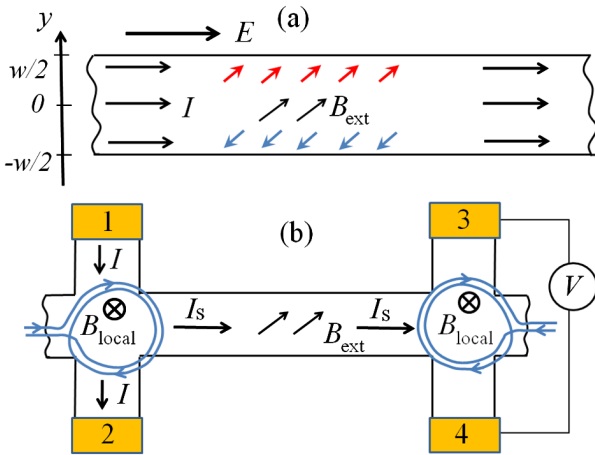


FIG. 2 (color online). (a) Schematic for spin accumulation in the SHE regime. An electric current in a graphene strip drives transverse spin current, resulting in spin density buildup across the strip, Eq. (3). (b) Generation and detection of spin current in the H geometry. Electric current passed through the region of local magnetic field drives spin current along the strip. Voltage generated via inverse SHE is detected using probes 3 and 4. Hanle-type oscillation due to spin precession can be induced by external magnetic field applied in plane.

to wavelength. This is true when the collision rate is small compared to typical particle energy, which requires weak disorder  $\gamma \ll k_B T$ , where  $\gamma$  is defined in Eq. (10), and small fine-structure parameter  $\alpha = e^2/\hbar v_0 \kappa \ll 1$  ( $\kappa$  is the dielectric constant).

The kinetic equation (5) can be solved analytically in the limit of small  $\alpha$  [25,26]. Rather than pursuing this route, we follow Ref. [27] to obtain transport coefficients from the balance of the net momentum for different groups of carriers, electrons, and holes, taken to be moving independently. We use a simple ansatz

$$f_{e(h)}(\mathbf{p}) = \frac{1}{e^{(\varepsilon_{\mathbf{p}} - \mathbf{p} \cdot \mathbf{a}_{e(h)} - \mu_{e(h)})/k_B T} + 1}, \quad \varepsilon_{\mathbf{p}} = v_0 |\mathbf{p}|, \quad (6)$$

where the chemical potentials satisfy  $\mu_e = -\mu_h$ , and the quantities  $\mathbf{a}_e$  and  $\mathbf{a}_h$  are introduced to describe a current-carrying state. This ansatz corresponds to a uniform motion of the electron and hole subsystems, such that the collision integral for the  $e$ - $e$  and  $h$ - $h$  processes vanishes. Thus only the  $e$ - $h$  collisions contribute to momentum relaxation, resulting in mutual drag between the  $e$  and  $h$  subsystems.

Equation (5) yields coupled equations for ensemble-averaged velocities and momenta of different groups of carriers (6):

$$q_i \left( \mathbf{E} + \frac{\mathbf{V}_i \times \mathbf{B}}{c} \right) = -\frac{\mathbf{P}_i}{\tau_i^{\text{dis}}} - \eta \sum_{i'} n_{i'} (\mathbf{V}_i - \mathbf{V}_{i'}), \quad (7)$$

where  $i, i'$  label the  $e$  and  $h$  subsystems with different spins. The ensemble-averaged scattering times  $\tau_i^{\text{dis}}$ , the carrier densities  $n_i$ , and the electron-hole drag coefficient  $\eta$  are specified below.

The quantities  $\mathbf{V}_i, \mathbf{P}_i$  are proportional to each other,  $\mathbf{P}_i = m_i \mathbf{V}_i$ . An explicit expression for  $m_i$  as a function of  $T, \mu$  can be found by expanding the distribution functions (6) to lowest nonvanishing order in  $\mathbf{a}_{e(h)}$ :

$$m_i = \frac{1}{v_0} \frac{\int d^2 \mathbf{p} p_x \nabla_{\mathbf{a}_x} f_i(\mathbf{p})}{\int d^2 \mathbf{p} (p_x/p) \nabla_{\mathbf{a}_x} f_i(\mathbf{p})} = \frac{1}{v_0} \frac{\int d^2 \mathbf{p} p_x^2 g_i(\mathbf{p})}{\int d^2 \mathbf{p} (p_x^2/p) g_i(\mathbf{p})}, \quad (8)$$

where  $g_i(\mathbf{p}) = f_i(\mathbf{p})[1 - f_i(\mathbf{p})]$ . The integrals over  $\mathbf{p}$ , evaluated numerically, give the effective mass as a function of  $T$  and  $\mu$ . At charge neutrality, setting  $\mu_{e(h)} = 0$ , we find  $m_T = \frac{9\zeta(3)}{2\zeta(2)} k_B T / v_0^2 \approx 3.29 k_B T / v_0^2$ .

The times  $\tau_i^{\text{dis}}$  and carrier densities  $n_i$  in (7) are expressed through the distribution function (6) with  $\mathbf{a}_i = 0$ :

$$\frac{1}{\tau_i^{\text{dis}}} = \frac{2}{n_i} \int \frac{d^2 \mathbf{p}}{(2\pi)^2} \frac{f_i(\mathbf{p})}{\tau_i^{\text{dis}}(\varepsilon_{\mathbf{p}})}, \quad n_i = 2 \int \frac{d^2 \mathbf{p}}{(2\pi)^2} f_i(\mathbf{p}), \quad (9)$$

where  $\tau^{\text{dis}}(\varepsilon)$  is the transport scattering time, Eq. (10), and the factor of 2 accounts for valley degeneracy.

We pick the model for disorder scattering to account for the experimentally observed linear dependence of conductivity versus doping,  $\sigma = \mu_* |n|$ , where  $\mu_*$  is the mobility away from the DP. This is the case for Coulomb impurities

or strong pointlike defects, such as adatoms or vacancies [13]. In both cases the scattering time has an approximately linear dependence on particle energy,

$$\tau^{\text{dis}}(\varepsilon)_{|\varepsilon| \gtrsim \gamma} = \hbar |\varepsilon| / \gamma^2, \quad \gamma = v_0 \sqrt{e \hbar / \mu_*}, \quad (10)$$

where the disorder strength parameter  $\gamma$  is expressed through mobility. The value  $\mu_* = 6 \times 10^4 \text{ cm}^2/\text{Vs}$  measured in graphene on BN [28] yields  $\gamma \approx 120 \text{ K}$ . Similar values are obtained from the  $\rho_{xx}$ -based DP width. Taking  $\Delta n \approx 10^{10} \text{ cm}^{-2}$  [20], we find  $\gamma \sim \hbar v_0 \sqrt{\Delta n} \approx 100 \text{ K}$ .

To obtain  $\rho_{xy}^{(l)}$ , we solve Eq. (7), accounting only for the drag between electrons and holes of the same spin. Including the drag between opposite spin species does not change the overall behavior of the transport coefficients and SHE [18]. Equation (7) can be conveniently analyzed using complex-valued quantities  $P_x + iP_y, V_x + iV_y$ , giving complex resistivity  $\tilde{\rho} = \rho_{xx}^{(l)} + i\rho_{xy}^{(l)}$ . We find

$$\tilde{\rho} = \frac{1}{e^2} \frac{m_e m_h \tilde{\gamma}_e \tilde{\gamma}_h + \eta n_e m_e \tilde{\gamma}_e + \eta n_h m_h \tilde{\gamma}_h}{n_e m_h \tilde{\gamma}_h + n_h m_e \tilde{\gamma}_e + \eta (n_e - n_h)^2}. \quad (11)$$

Here  $\tilde{\gamma}_i = \frac{1}{\tau_i^{\text{dis}}} - i\Omega_i$ , with  $\Omega_i = q_i B / m_i c$  the cyclotron frequency.

As a consistency check, we consider the behavior at charge neutrality. Setting  $n_e = n_h, m_e = m_h$ , etc. gives  $\rho_{xx}$ , which is a sum of the Drude-Lorentz resistivity and the electron-hole drag contribution analyzed in Refs. [25,26],

$$\rho_{xx}^{(l)} = \frac{m_T}{2n_T e^2 \tau} (1 + \tau^2 \Omega^2) + \frac{\eta}{e^2}, \quad n_T = \frac{\pi k_B^2 T^2}{12 \hbar^2 v_0^2}, \quad (12)$$

and  $\rho_{xy}^{(l)} = 0$ . Here  $n_T$  is the density of thermally activated electrons (holes) at the DP, having fixed spin projection. Disorder scattering (first term) dominates at low temperatures  $T \lesssim T_* = \gamma \sqrt{\hbar/\eta}$  (at  $B = 0$ ), while electron-hole drag (last term) dominates at  $T \gtrsim T_*$ .

The value  $\eta$  can be obtained by matching the last term in Eq. (12), divided by 2 to account for spin, to the analytic result  $\rho_{xx} \approx 8.4 \hbar \alpha^2 / e^2$  [25,26]. We evaluate  $\alpha$  using the effective dielectric constant  $\kappa = \frac{\varepsilon_0 + 1}{2} + \frac{\pi}{2} \frac{e^2}{\hbar v_0} \approx 6$ , which accounts for intrinsic screening in the RPA approximation. Taking  $\varepsilon_0 \approx 4$  for BN substrate [28] yields  $\alpha \approx 0.37$ , giving  $\eta \approx 2.3 \hbar$ .

The dependence of transport coefficients on  $T, B$ , and carrier density  $n$ , predicted from Eq. (11), can be directly compared to experiment. Figure 3 shows  $\rho_{xy}(n)$  measured in graphene on BN, on samples similar to those described in Ref. [20]. The modeled  $\rho_{xy}(n)$  captures the main features of the data: the  $1/n$  dependence at large  $n$  and a steep linear dependence near the DP. The linear region broadens with temperature at  $T \gtrsim \gamma$ . The peak in  $\rho_{xx}(n)$  features similar thermal broadening [18]. The SHE coefficient, found from Eq. (3), is plotted in Fig. 1.

We now explore the behavior of transport coefficients near the DP, making estimates separately for  $T \gtrsim T_*$  and  $T \lesssim T_*$ . This can be conveniently done using an



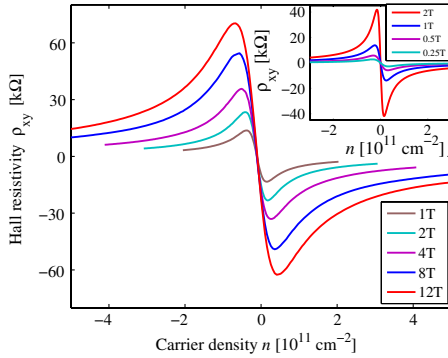


FIG. 3 (color online). Measured  $\rho_{xy}(n)$  for a high-mobility graphene sample on BN substrate at  $T = 250$  K. The dependence follows the quasiclassical formula (1) away from the DP, and is linear with a steep slope near the DP. Inset: Results for  $\rho_{xy}(n)$  obtained from the two-carrier model, Eqs. (7) and (11), for disorder strength  $\gamma = 180$  K found by fitting the distance between the maximum and the minimum in measured  $\rho_{xy}$  for  $B = 1$  T. Other parameters are  $\eta = 2.3\hbar$ ,  $T = 250$  K.

interpolation formula  $\tau_i^{\text{dis}}(\mu, T) = m_i(\mu, T)v_0^2\hbar/\gamma^2$  which links the ensemble-averaged scattering time (9) and the effective mass (8) in the entire range of  $T$  and  $\mu$  of interest.

We find the slope of  $\rho_{xy}$  at the DP by expanding Eq. (11) in small  $n = n_e - n_h$  [18]. The result can be described by a single interpolation formula,

$$\left. \frac{\partial \rho_{xy}}{\partial n} \right|_{n=0} = \frac{\hbar^2 v_0^2}{\min(T_*, \pi T^2/3)} \frac{B}{n_T e c}, \quad (13)$$

where only terms first order in  $B$  have been retained.

The SHE coefficient, Eq. (3), found by combining the results (13) and (12), and using thermally broadened density of states at the DP  $\partial n/\partial \mu = \frac{2\ln 2}{\pi} \frac{k_B T}{\hbar^2 v_0^2}$  [18], is

$$\theta_{\text{SH}}|_{n=0} = \frac{\lambda E_0^2 E_Z}{2\gamma^2 k_B T}, \quad E_0 = v_0 \sqrt{2\hbar e B/c}, \quad (14)$$

where  $E_0$  is the cyclotron energy. The functional form is the same in both regimes,  $\theta_{\text{SH}} \propto B^2/T$ , with different prefactors  $\lambda_{T \gtrsim T_*} = 24 \ln 2/\pi^2$  and  $\lambda_{T \lesssim T_*} = 12 \ln 2/\pi^2$ . The  $1/T$  growth of  $\theta_{\text{SH}}$  saturates at  $k_B T \approx \gamma$ , reaching maximum value  $\theta_{\text{SH}, \text{max}} \approx \frac{1}{2} \lambda E_0^2 E_Z/\gamma^3$ .

We expect suspended graphene [29,30] to feature an even stronger SHE than graphene on BN. Using typical mobility  $\mu_* = 2 \times 10^5 \text{ cm}^2/\text{Vs}$  [30], we estimate  $\gamma \sim 65$  K, whereas the temperature dependence of the conductivity at the DP [30] yields  $\gamma \sim 10$  K. For either value of  $\gamma$ , Eq. (14) predicts very large values  $\theta_{\text{SH}}$  at the DP.

Based on these estimates, we expect strong SHE response already at moderate fields  $B \lesssim 1$  T. Besides spin accumulation and locally tunable SHE response, which was discussed above, SHE can also manifest itself in a nonzero Hall voltage in response to spin-polarized currents injected from magnetic contacts.

Since our SHE mechanism does not rely on the relativistic dispersion of excitations, it can also be realized in

other zero-gap semiconductors (e.g., graphene bilayer) or in half-metals, materials with spin-polarized conduction band. It also applies, with suitable modifications, to the valley degrees of freedom in graphene. It was predicted that a (nonquantizing) magnetic field can produce a Zeeman-like valley splitting [31]. This will imbalance the Hall resistivities and result in a valley-Hall effect of a magnitude similar to the SHE.

We thank D. Goldhaber-Gordon, L. M. K. Vandersypen, and M. Soljacic for useful discussions and acknowledge support from Naval Research Grant No. N00014-09-1-0724 (L. L.) and Aspen Center for Physics (D. A.).

- [1] M. I. Dyakonov and V. I. Perel, *Sov. Phys. JETP Lett.* **13**, 467 (1971).
- [2] J. E. Hirsch, *Phys. Rev. Lett.* **83**, 1834 (1999).
- [3] S. A. Wolf *et al.*, *Science* **294**, 1488 (2001).
- [4] Y. K. Kato *et al.*, *Science* **306**, 1910 (2004).
- [5] J. Sinova *et al.*, *Phys. Rev. Lett.* **92**, 126603 (2004).
- [6] N. Tombros *et al.*, *Nature (London)* **448**, 571 (2007).
- [7] S. Cho, Y.-F. Chen, and M. S. Fuhrer, *Appl. Phys. Lett.* **91**, 123105 (2007).
- [8] W. Han *et al.*, *Phys. Rev. Lett.* **105**, 167202 (2010).
- [9] D. Huertas-Hernando, F. Guinea, and A. Brataas, *Phys. Rev. B* **74**, 155426 (2006).
- [10] C. Józsa *et al.*, *Phys. Rev. B* **80**, 241403(R) (2009).
- [11] K. Pi *et al.*, *Phys. Rev. Lett.* **104**, 187201 (2010).
- [12] D. Huertas-Hernando, F. Guinea, and A. Brataas, *Phys. Rev. Lett.* **103**, 146801 (2009).
- [13] A. H. Castro Neto and F. Guinea, *Phys. Rev. Lett.* **103**, 026804 (2009).
- [14] C. Ertler *et al.*, *Phys. Rev. B* **80**, 041405(R) (2009).
- [15] H. Min *et al.*, *Phys. Rev. B* **74**, 165310 (2006).
- [16] C. L. Kane and E. J. Mele, *Phys. Rev. Lett.* **95**, 226801 (2005).
- [17] D. A. Abanin, P. A. Lee, and L. S. Levitov, *Phys. Rev. Lett.* **96**, 176803 (2006).
- [18] See Supplemental Material at <http://link.aps.org/supplemental/10.1103/PhysRevLett.107.096601> for details of the transport model.
- [19] D. A. Abanin *et al.*, *Phys. Rev. Lett.* **98**, 196806 (2007).
- [20] D. A. Abanin *et al.*, *Science* **332**, 328 (2011).
- [21] I. Meric *et al.*, *Nature Nanotech.* **3**, 654 (2008).
- [22] C. L. Degen *et al.*, *Proc. Natl. Acad. Sci. U.S.A.* **106**, 1313 (2009).
- [23] E. M. Hankiewicz *et al.*, *Phys. Rev. B* **70**, 241301(R) (2004).
- [24] D. A. Abanin *et al.*, *Phys. Rev. B* **79**, 035304 (2009).
- [25] A. B. Kashuba, *Phys. Rev. B* **78**, 085415 (2008).
- [26] L. Fritz *et al.*, *Phys. Rev. B* **78**, 085416 (2008).
- [27] V. F. Gantmakher and Y. B. Levinson, *Zh. Eksp. Teor. Fiz.* **74**, 261 (1978) [*Sov. Phys. JETP* **47**, 133 (1978)].
- [28] C. R. Dean *et al.*, *Nature Nanotech.* **5**, 722 (2010).
- [29] X. Du *et al.*, *Nature Nanotech.* **3**, 491 (2008).
- [30] K. I. Bolotin *et al.*, *Solid State Commun.* **146**, 351 (2008).
- [31] I. A. Luk'yanchuk and A. M. Bratkovsky, *Phys. Rev. Lett.* **100**, 176404 (2008).